Mon. Not. R. Astron. Soc. **000**, 1–13 (2013) Printed 20 February 2014 (MN LATEX style file v2.2)

Active Galactic Nuclei-driven outflows without quenching in simulations of high-redshift disk galaxies

J. M. Gabor,[1⋆] Frédéric Bournaud[1]
[1] *CEA-Saclay, IRFU, SAp, F-91191 Gif-sur-Yvette, France*

arXiv:1402.4482v1 [astro-ph.CO] 18 Feb 2014

20 February 2014

ABSTRACT

Recent observations have revealed nuclear outflows in high-redshift, star-forming galaxies. We study outflows driven by Active Galactic Nuclei (AGNs) using high-resolution simulations of idealized $z \sim 2$ isolated disk galaxies. Episodic accretion events lead to outflows with velocities > 1000 km s^{-1}and mass outflow rates up to the star formation rate (several tens of $M_\odot$ yr^{-1}). Outflowing winds escape perpendicular to the disk with wide opening angles, and are typically asymmetric (i.e. unipolar) because dense gas above or below the AGN in the resolved disk inhibits outflow. Owing to rapid variability in the accretion rates, outflowing gas may be detectable even when the AGN is effectively "off." The highest velocity outflows are concentrated within $2-3$ kpc of the galactic center during the peak accretion. With our purely thermal AGN feedback model – standard in previous literature – the outflowing material is mostly hot ($\gtrsim 10^6$ K) and diffuse ($n_H \lesssim 10^{-2}$ cm^{-3}), but includes a cold component entrained in the hot wind. Despite the powerful bursts and outflow rates near the star formation rate, AGN feedback has little effect on the dense gas in the galaxy disk.

Key words: galaxies:evolution – galaxies:formation – galaxies:nuclei – galaxies:high-redshift – galaxies:active

1 INTRODUCTION

Many models of the co-evolution of galaxies and supermassive black holes (BHs) invoke active galactic nuclei (AGN)-driven winds to regulate black hole growth and impact the host galaxy (e.g. Ciotti & Ostriker 1997; Haehnelt et al. 1998; Silk & Rees 1998; Fabian 1999; Ciotti & Ostriker 2001; Wyithe & Loeb 2003; Begelman & Nath 2005; Di Matteo et al. 2005; Sazonov et al. 2005; Springel et al. 2005; King 2005; Hopkins et al. 2006; Robertson et al. 2006; Somerville et al. 2008; Ciotti et al. 2010; King 2010b,a; Dubois et al. 2010a; Novak et al. 2011; Teyssier et al. 2011; Debuhr et al. 2012; Dubois et al. 2012; Martizzi et al. 2012; Dubois et al. 2013a,b). Such outflows may help establish correlations between the black hole and galaxy properties (e.g. Kormendy & Richstone 1995; Magorrian et al. 1998; Richstone et al. 1998; Ferrarese & Merritt 2000; Gebhardt et al. 2000; McLure & Dunlop 2002; Tremaine et al. 2002; Marconi & Hunt 2003; Treu et al. 2004; Peng et al. 2006; Graham 2007; Treu et al. 2007; Jahnke et al. 2009; Bennert et al. 2011; Canalizo et al. 2012; Graham & Scott 2013; Kormendy & Ho 2013). Quasar winds may help expel sufficient quantities of gas from their host galaxies to regulate their star-formation, and in this way suppress the stellar mass growth of high-mass galaxies.

Motivated in part by models with quasar outflows, observations have begun to probe galaxy-scale outflows possibly driven by AGN feedback (Tremonti et al. 2007; Feruglio et al. 2010; Alatalo et al. 2011; Lehnert et al. 2011; Nesvadba et al. 2011; Rupke & Veilleux 2011; Aalto et al. 2012; Cicone et al. 2012; Cano-Díaz et al. 2012; Harrison et al. 2012; Maiolino et al. 2012; Cicone et al. 2013; Förster Schreiber et al. 2013; González-Alfonso et al. 2013; Rupke & Veilleux 2013; Spoon et al. 2013; Veilleux et al. 2013). Outflows are detected in both ionized and molecular gas, and from the local Universe up to $z \sim 2$. The highest velocities are often found along lines-of-sight near the galactic nucleus, and these velocities ($\gtrsim 10^3$ km s^{-1}) seem to be higher than those caused by stellar feedback. These high velocities and central locations are frequently used to argue that the outflows are powered by AGN rather than supernovae or young stars. With some assumptions, mass outflow rates are estimated at ~ 100 $M_\odot$ yr^{-1}or sometimes even higher, or a few times the star-formation rate (SFR; e.g. Cicone et al. 2013; Förster Schreiber et al. 2013).

Some authors suggest that the observed AGN-driven outflows are quenching star-formation in their host galaxies by expelling the gas, yet most host galaxies

⋆ Email:jared.gabor@cea.fr

are still forming stars. Most observed AGNs occur in undisturbed star-forming disk galaxies up to redshift $z \sim 2$ (Grogin et al. 2005; Pierce et al. 2007; Gabor et al. 2009; Georgakakis et al. 2009; Silverman et al. 2009; Cisternas et al. 2011; Kocevski et al. 2012; Mullaney et al. 2012; Rosario et al. 2012; Schawinski et al. 2012; Simmons et al. 2012; Juneau et al. 2013), although especially luminous or obscured AGNs may be more likely to be hosted by merging galaxies (Bennert et al. 2008; Cales et al. 2011; Bessiere et al. 2012; Ramos Almeida et al. 2012; Treister et al. 2012; Juneau et al. 2013; Hopkins et al. 2013). It remains unclear whether moderate-luminosity AGNs in disk galaxies can drive outflows or have a major impact on the evolution of their host galaxies. Observed outflows attributed to AGN in fact sometimes occur in galaxies with little or no indications of current AGN (Tremonti et al. 2007; Förster Schreiber et al. 2013).

In Gabor & Bournaud (2013b) we presented simulations of gas-rich, isolated disk galaxies whose supermassive black holes accrete significantly. Accretion is highly variable, with stochastic $\sim$ 10 Myr episodes of Eddington-limited accretion. In the present paper, we show that these high-accretion episodes generate powerful AGN outbursts, driving hot, high-velocity outflows from the galaxy. The outflow rates peak near the SFR, but the outflows have little overall effect on the gas in the galactic disk. We summarize our simulation methods in §2, describe our results in §3, and discuss caveats and implications in §4. We conclude with §5.

2 SIMULATIONS

The simulations used in this work use the same methods as Gabor & Bournaud (2013b). The simulations are described fully there, and we summarize them here.

We use a customized version of the Adaptive Mesh Refinement (AMR) hydrodynamics code Ramses[1] (Teyssier 2002), which solves the equations of hydrodynamics and N-body dynamics on a cubic grid whose cells can vary in size. We start with an initial uniform grid of 256^3 cells in a 50 kpc box and refine to smaller cells when the mass in a cell exceeds a given threshold, or the gas Jeans length becomes smaller than 4 times the cell size. We allow refinement up to a maximum resolution (i.e. minimum cell size) of ≈ 6 pc.

The code includes models for cooling, star-formation, supernova feedback, and black hole growth and feedback. Cooling acts as a sink term for the thermal energy of the gas (although gas may actually gain energy due to heating from a uniform UV background Katz et al. 1996; Sutherland & Dopita 1993). We allow gas to cool to 100 K, except that we use a density-dependent temperature floor at high densities to ensure the local Jeans length is always resolved by at least four grid cells (Truelove et al. 1997).

In gas cells with density $n_H > 100$ cm^{-3} stars form with a star-formation rate density of $\dot{\rho}_* = 0.01\rho_{\rm gas}/t_{\rm ff} \propto \rho_{\rm gas}^{1.5}$ (Rasera & Teyssier 2006), where $\rho_{\rm gas}$ is the mass density of gas in the cell, $t_{\rm ff}$ is the free-fall time of the gas, and 0.01 is the star-formation efficiency parameter (Krumholz & Tan 2007). New collisionless star particles are stochastically spawned in eligible gas cells with a probability appropriate for the star-formation rate.

Ten Myr after each star particle is formed, twenty per cent of its initial mass explodes as supernovae. Supernova explosions are modeled by adding thermal energy to the gas cell in which the star particle lives. For each 10 M$_\odot$ which explodes as supernovae, 10^{51} ergs are added to the host gas cell's thermal energy. Cooling is delayed for the heated cell for 2 Myrs to prevent the injected energy from being radiated away too quickly (cf. Stinson et al. 2006; Teyssier et al. 2013; Perret et al. 2013). This simple stellar feedback model regulates the structure of the interstellar medium and suppresses star-formation. Although the stellar feedback generates turbulence and thickens the disk, it drives only weak winds that typically have velocities below the escape speed of the galaxy. Star-forming clumps throughout the galactic disk launch outflows locally. The weakness of the stellar-driven winds, combined with the fact that they are launched throughout the disk, allows us to isolate the effects of AGN-driven winds in this work. If anything, the stellar outflows may have second-order effects on the long-range propagation of AGN outflows by changing the gas density and temperature into which AGN-driven shocks propagate. We control for such effects in our analysis by comparing simulations with and without AGN, finding that stellar-driven outflows are typically $\sim 10\times$ weaker than AGN-driven outflows. More sophisticated stellar feedback models (which we will examine in future work; e.g. Renaud et al. 2013) lead to efficient outflows without AGN, but an ISM structure that is similar to the simulations we use here (Hopkins et al. 2012c; Bournaud et al. 2014; Perret et al. 2013).

We model a central supermassive black hole as a sink particle (Krumholz et al. 2004; Dubois et al. 2010a; Teyssier et al. 2011). We calculate the Bondi accretion rate $\dot{M}_{\rm BH} = (4\pi G^2 M_{\rm BH}^2 \rho)/((c_s^2 + u^2)^{3/2})$ (Bondi & Hoyle 1944; Bondi 1952; Hoyle & Lyttleton 1939) by measuring the gas density ρ, sound speed c_s, and relative velocity u within a sphere of radius $4dx$, where dx is the smallest resolution element. This accretion rate is capped at the Eddington limit (cf. Eddington 1916) $\dot{M}_{\rm Edd} = (4\pi G M_{\rm BH} m_p)/(\epsilon_r \sigma_T c)$, where m_p is the proton mass, σ_T is the Thomson scattering cross-section, c is the speed of light, and $\epsilon_r = 0.1$ is the efficiency with which accreted mass is converted into luminous energy. During each time step the sink particle mass increases and an equivalent mass is removed from the local gas cells according to the accretion rate.

The amount of mass accreted by the black hole is stored as a variable, and the corresponding energy may be released as AGN feedback during coarse timesteps (those that correspond to the coarsest-resolution cells). As above, we assume that 10 per cent of the accreted mass is converted into luminous energy and 15 per cent of the luminous energy couples to the gas as thermal energy (Dubois et al. 2012). If the accreted mass is sufficient to heat the gas within a radius of $4dx$ to 10^7 K, then we inject the energy; if not, then we "store" the accreted mass and check again at the following coarse time step after additional mass has been accreted. Storing the accreted mass assures that AGN feedback energy is only injected at temperatures above 10^7 K and thus that the injected energy is not rapidly radiated away (Booth & Schaye 2009). This allows thermal energy injection to develop efficient pressure-driven outflows. We

[1] `http://www.itp.uzh.ch/~teyssier/Site/RAMSES.html`

also enforce an upper limit to the gas temperature after energy injection of 5×10^9 K to prevent unphysically high temperatures. If the energy is sufficient to heat the nearby gas above this temperature, we iteratively expand the injection region until the post-injection temperature drops below this value.

We construct initial conditions for each isolated disk galaxy with collisionless star particles in an exponential disk plus bulge, dark matter particles for the central regions of a dark matter halo, and an exponential gas disk. We place a black hole with a mass consistent with the local $M_{\rm BH} - M_{\rm bulge}$ (Bennert et al. 2011) relation at the galactic center. The circum-galactic gas is set to a uniform, low density, 5×10^{-4} of the gas density at the edge of the galactic disk, or $\sim 10^{-5}$ cm^{-3}, and it has a temperature of $\sim 10^{5.5}$ K. We allow the initial conditions to relax both before starting the Ramses simulation, and during the first $100 - 300$ Myr of evolution with Ramses at low resolution to suppress any spurious density waves.

In Gabor & Bournaud (2013b) we presented six main simulations: three gas-rich (~ 50 per cent gas fractions) star-forming disks representing $z \gtrsim 2$ main sequence galaxies, and three low-gas fraction (10 per cent) star-forming disks representing low-redshifts galaxies. We found little black hole growth and low accretion rates in the low-redshift simulations. Our focus in this paper is the high-redshift, gas-rich regime, where black holes grow substantially and accrete at the Eddington limit for episodes lasting ~ 10 Myr at a time.

The simulated galaxies have baryonic masses of $1 \times 10^{10}, 4 \times 10^{10}$, and 16×10^{10} M$_\odot$, and we name the runs M1f50, M4f50, and M16f50 accordingly (where e.g. "M16" refers to the baryonic mass and "f50" refers to the gas fraction). All simulations begin with gas fractions > 50 per cent so that, even after gas consumption due to star-formation, they remain ≈ 50 per cent during the ~ 100 Myr high-resolution portion of the runs. In the figures we will show mostly results from simulation M4f50, which has the most intense black hole accretion history and thus the most spectacular outflows. We have re-run this simulation with a higher frequency of output snapshots to enhance the analysis, and the new version differs from the old only in slight details due to stochasticity in the simulations. We will draw conclusions based on all three simulations. In Gabor & Bournaud (2013b) we also discussed a simulation with no AGN feedback that is otherwise identical to simulation M4f50. The two simulations (with and without AGN feedback) start from the same initial conditions and undergo the same relaxation procedure. Here we use the "no AGN feedback" simulation to isolate winds driven by the AGN rather than supernovae, and to gauge the effect of AGN feedback on the host galaxy.

Using these high gas fraction simulations in Gabor & Bournaud (2013b), we found that dense gas clouds in the turbulent disk interact and exchange angular momentum, stochastically converging toward the galaxy center and fueling the black hole (cf. Hopkins & Hernquist 2006; Dekel et al. 2009; Ceverino et al. 2010; Bournaud et al. 2011). Black hole accretion is variable on ~ 1 Myr timescales due to structure in the ISM, and the dense clouds trigger ~ 10 Myr episodes of Eddington-limited accretion. Occasionally reaching the quasar level (up to $\sim 10^{46}$ erg s^{-1}), the corresponding AGN luminosities scale with the SFR as in observations (Rosario et al. 2012). The black hole growth – dominated by the high-accretion rate episodes – can explain the black hole growth required to remain on the $M_{\rm BH} - M_{\rm bulge}$ relation. Thus the stochastic migration of dense clouds can fuel an AGN in isolated, gas-rich disk galaxies. In the remainder of this work, we study the outflows generated by such AGN.

3 SIMULATION RESULTS

3.1 AGN outflows in bursts

In Gabor & Bournaud (2013b) we showed that black hole accretion rates are highly variable, with brief episodes of Eddington-limited accretion. The variability is driven by the turbulent structure of the ISM, and the high-accretion episodes are triggered when a dense cloud stochastically collides with the black hole. High-accretion episodes typically last for $\sim 5 - 10$ Myr.

During high-accretion episodes, the black hole injects powerful bursts of thermal energy into the immediately surrounding gas, and the super-heated gas expands and shocks the gas in its path. Figure 1 shows two examples of AGN outbursts in our simulations through ~ 10 Myr time-series of snapshots (with time increasing from left to right). The figure shows an edge-on view of the galaxy disk in temperature (top row, red), gas density (middle row, green), and outflow velocity (bottom row, blue), all mass-weighted along the line-of-sight. The outflow velocity shown is only the vertical $z-$direction, perpendicular to the disk plane. In each panel a blue plus sign indicates the location of the black hole in the center of the galaxy.

The first AGN outburst (top three rows in Figure 1) expands in a shock above the plane of the disk. The shock front is nearly semi-spherical. The outburst does not expand below the disk because dense structures in the ISM that are close the to black hole block it. The shock hits dense gas clouds that absorb the energy and efficiently radiate it away.

The outflow develops primarily as a hot ($> 10^7$ K), low-density ($n_H \lesssim 10^{-2}$) expansion, but the hot gas entrains colder, denser clouds as well. One such cloud is visible as a darker clump in the density map above the disk at 16.9 Myr. These swept-up clouds are not as cold and dense as star-forming clumps in the galactic disk. We discuss the phase structure of outflows further in §3.3.

After the outburst launches, the shock wave propagating out of the disk remains visible for ~ 10 Myr, maintaining high velocities throughout this time. This timescale is comparable to, and sometimes longer than, the time during which the black hole accretion rate remains high. Since the outflow takes several Myr to propagate to large distances, it does not fully reflect the rapid variability of accretion rates. Thus the AGN-driven outflows may be detectable even while the AGN is "off" (see §3.2).

The second AGN outburst (bottom three rows in Figure 1) actually comprises a series of consecutive bursts. Each successive burst creates a new shock front expanding in a shell, leading to an appearance of nested shock shells (e.g. at 78.5 Myr, most obvious in temperature). Once again the outburst is asymmetric, with most of the outflow escaping below the disk and little above it. Dense clouds are entrained

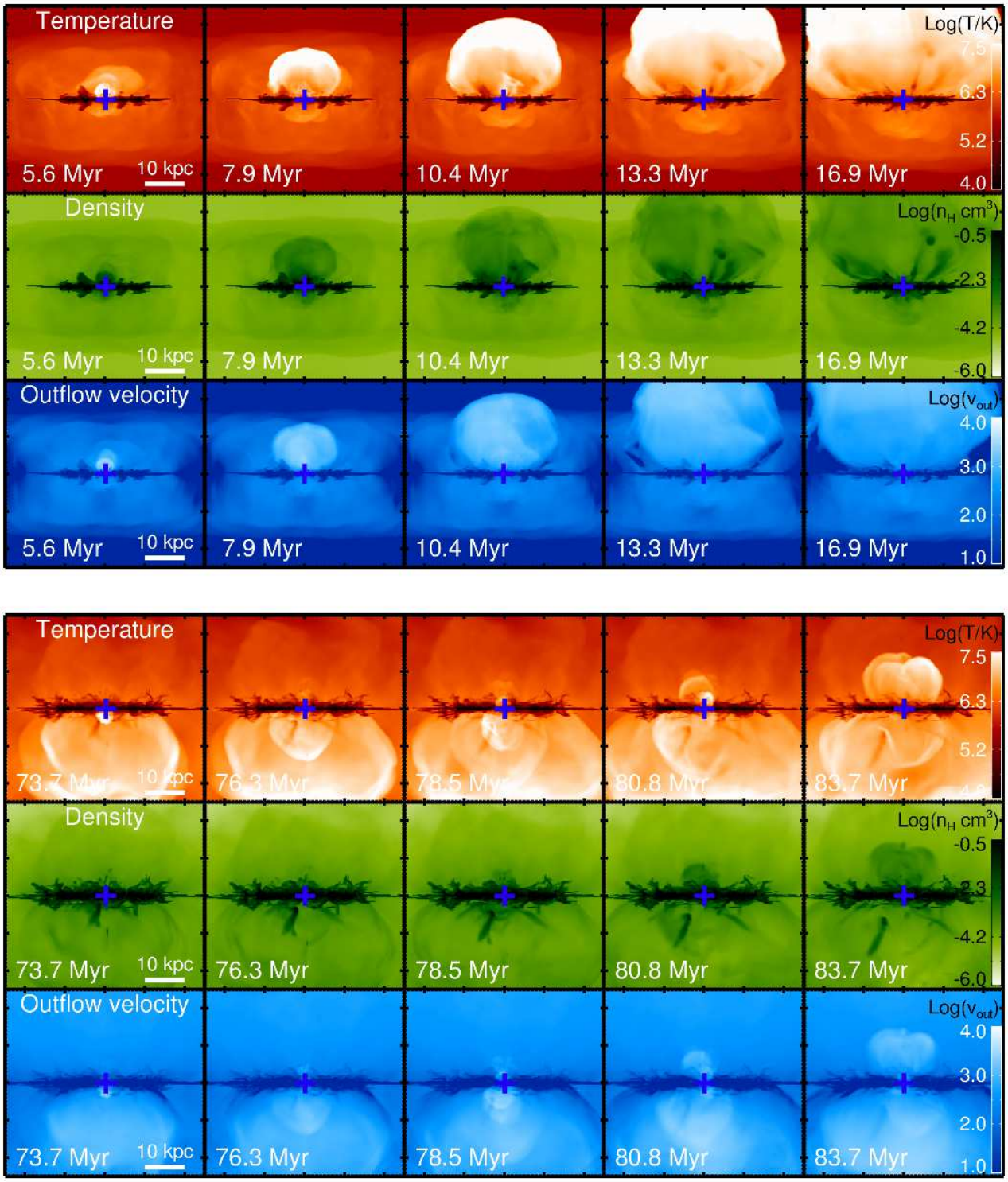

Figure 1. Edge-on view of a simulated galaxy disk showing AGN-driven outflow bursts. The top three rows show a single powerful burst in a time sequence between 5.6 and 17 Myr, while the bottom three rows show multiple bursts between 73.7 and 83.7 Myrs. For each set, the top panels show gas temperature (red scale), middle panels show gas number density n_H (green scale), and bottom panels show the outflow velocity perpendicular to the disk (blue scale). In both examples, an AGN outburst heats gas to $> 10^7$ K, generating a shock that propagates outward from the disk. The hot, low-density shock front expands at > 1000 km s^{-1}, entraining colder denser clouds. The outbursts are frequently asymmetric because dense clouds within the disk effectively block the outflows in some directions. The gas disk remains intact.

in the hot outflow, and a bow shock is visible along the edge of an outflowing cloud closest to the galactic disk.

In both cases, the AGN outbursts apparently leave the galaxy disk intact – most of the cold, dense gas appears to remain in the disk. We return to this point in §3.5.

In summary, episodes of high black hole accretion generate brief, powerful bursts of AGN feedback. Repeated accretion events lead to repeated, distinct outbursts. The AGN-heated, 10^7 K gas expands away from the gas disk as a shock at > 1000 km s^{-1}, sweeping up cooler, denser clouds along the way. The high-density clouds of the ISM are able to halt the shock in its path, generally leading to asymmetric outflows since the outflow in one direction may be blocked. The gas disk of the galaxy is not destroyed or disrupted by the outbursts. In the following sections we examine in further detail the outflow rates, the phase structure of the outflows, and effects on the galaxy.

3.2 Mass outflow rates

Figure 1 above indicates that AGN feedback generates hot, high-velocity outflows. To help understand the broader impact of AGN on galaxies and their evolution, we measure the mass outflow rates in our simulations.

We estimate instantaneous outflow rates through planes above and below the galaxy disk. Our fiducial planes are 3 kpc above and 3 kpc below the disk. For every cell in the simulation box at a given snapshot, we determine whether its $z-$velocity would cause it to cross the plane within the next $\Delta t = 1$ Myr. If so, and if it is moving outward from the disk, we count its mass toward the total mass outflow, $\Delta M_{\rm out}$. We also measure mass inflows but these are typically a factor of 10 smaller. The mass outflow rate is then estimated using $\dot{M}_{\rm out} = \Delta M_{\rm out}/\Delta t$. Different choices of Δt change the outflow rates at the ~ 10 per cent level.

We show the mass outflow rates in the top panel of Figure 2. As pointed out above, outflows have a bursty history, following from the episodic accretion history. For comparison, we show the accretion rate history in the bottom panel of Figure 2. Brief periods of Eddington-limited accretion generally lead to brief periods of high outflow rates. The accretion variability timescale, however, is sometimes shorter than the timescale for outflows to propagate to our measurement plane at 3 kpc. Thus there is not an exact one-to-one correspondance between intantaneous accretion rate and intantaneous outflow rate, and outflow rates vary more slowly. This effect also allows for substantial outflow rates when the AGN appears to be "off," as in some observations (e.g. Förster Schreiber et al. 2013).

The outflow rates shown in Figure 2 peak around 30 M$_\odot$ yr^{-1}. Despite that the outflows are hot and mostly low-density gas, the peak outflow rates are similar to the SFR in the simulation (shown as a dotted line). The peak outflow rates are also about two orders of magnitude greater than the black hole accretion rate. Due to the bursty accretion history, the outflows reach these peak rates only for short periods of time. After the outburst, outflow rates quickly fall to lower values around ~ 5 M$_\odot$ yr^{-1}. During active phases of the AGN, the average outflow rate is about half the peak rate, ~ 15 M$_\odot$ yr^{-1}or the SFR/2. We also show the mean outflow rate over the 100 Myr simulation as a dashed line, and it is about 10 M$_\odot$ yr^{-1}, or one-third

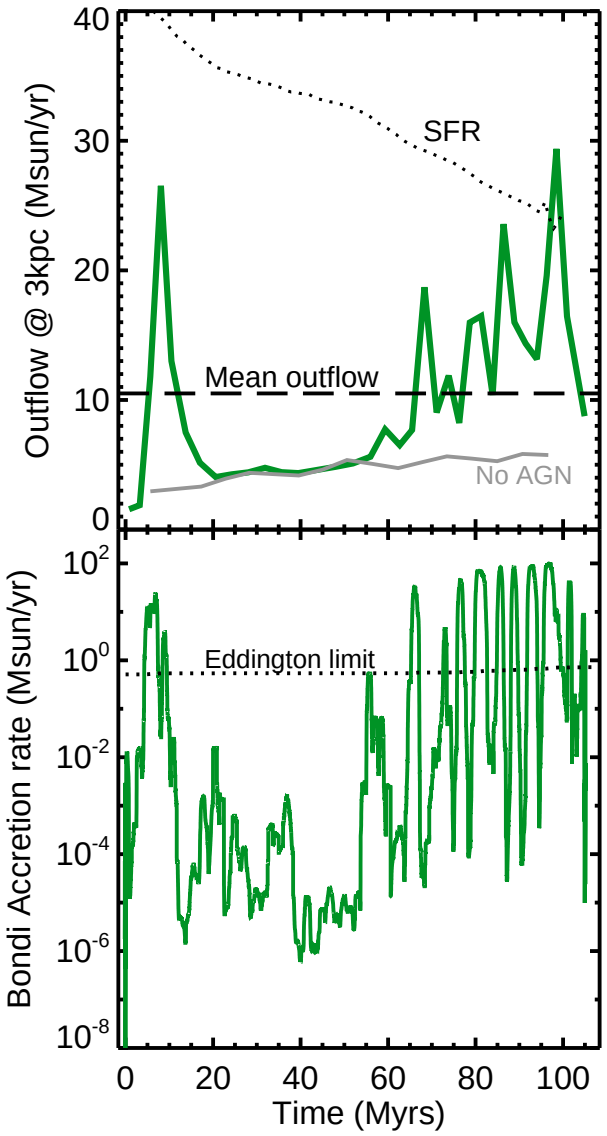

Figure 2. Top: Mass outflow rate through a plane 3 kpc above (and below) the galactic disk, as a function of time (solid green). A dashed horizontal line shows the mean outflow rate during this period, and the dotted line shows the SFR for comparison. **Bottom:** Bondi black hole accretion rate as a funciton of time, with the Eddington limit shown as a dotted line. The actual accretion rate of the black hole is capped at the Eddington limit. Peaks in the accretion rate lead to outflows in bursts with rates comparable to the SFR. The time-variability of the outflows lags that of the accretion rate because it takes ~ 1 Myr for outflows to propagate from the nucleus to 3 kpc.

the star-formation rate. For comparison, our simulation with no AGN feedback has a relatively constant outflow rate of $3-5$ M$_\odot$ yr^{-1}driven by stellar feedback.

In our more massive simulated galaxy, M16f50, the black hole accretion is dominated by a single event near the Eddington-limit. The outflow rate peaks around 30 M$_\odot$ yr^{-1}during this event, with a mean outflow rate ~ 10 M$_\odot$ yr^{-1}. This outflow rate is similar to those found in our medium-mass simulation (cf. Figure 2). In our least mas-

sive simulated galaxy, M1f50, the outflows are dominated by a single, longer outburst lasting for ~ 20 Myr and peaking at 10 $M_\odot$ yr^{-1}, or about $2-3\times$ the SFR. There may be trends between outflow rates and black hole mass and galaxy disk mass, but any such trends are too weak to conclusively glean from our small number of simulations.

In summary, high mass outflow rates follow rapidly after high-accretion events, as AGN feedback during Eddington-limited growth episodes drives high-velocity winds. Since black hole accretion is rapidly varying, so too are outflow rates. But the time lag for outflows to propagate from the black hole vicinity to the measurement plane (3 kpc) causes the outflow rates to be less variable than accretion rates. The peak mass outflow rates are of order the galaxy's star-formation rate, or in our main example, ≈ 30 $M_\odot$ yr^{-1}. The peak outflow episodes are brief, however, and outflow rates rapidly return to lower values. For our simulation with the most active accretion history, the mean outflow rate is about 10 $M_\odot$ yr^{-1}, or one-third the star-formation rate.

3.3 Density and temperature of AGN outflows

Based on Figure 1 we suggested that the outflows are primarily hot and low-density, but some colder, denser clouds are entrained in the flow. The temperature and density structure of outflows will determine whether and how observations can detect them – hot gas may be detectable in X-rays or from ionization lines, while cold dense gas may be detected via molecular line observations. The phase structure also influences how outflows propagate into a realistic circum-galactic and intergalactic medium. In this section we explicitly study the temperature and density of our simulated AGN-driven outflows.

Figure 3 shows the gas temperature (top panel) and density (bottom panel) as a function of velocity for outflowing gas for one snapshot of a simulation during a powerful outburst. The color of each pixel indicates the mass of gas at that pixel's temperature and velocity, in $M_\odot$. The velocities reach ≈ 5000 km s^{-1}. Most of the high-velocity outflows have a temperature between 10^6 and 10^8 K, but outflows up to ~ 1000 km s^{-1}have temperatures between 10^4 and 10^6 K, and some outflowing gas is at the temperature floor of our simulation, 10^2 K. Likewise, most of the high-velocity outflowing gas is diffuse with $n_H < 10^2$ cm^{-3}, but some outflowing gas has densities $n_H > 10^{-1}$ cm^{-3}. Little or no outflowing gas has densities $> 10^2$ cm^{-3}, so molecular outflows would be rare unless the cold clouds in our simulation could form sub-resolution molecular clouds.

In summary, most of the high-velocity (up to 5000 km s^{-1}) outflowing gas is hot and diffuse, with temperatures of $10^6 - 10^8$ K and densities $10^{-4} - 10^{-2}$ cm^{-3}. Some of the outflowing gas, however, has temperatures as low as our simulation's temperature floor (100 K), and densities $> 10^{-1}$ cm^{-3}.

3.4 Line-of-sight dependence of outflow

Observers sometimes attribute galactic outflows to AGNs because outflow velocities are higher close (in projection) to the galactic nucleus (e.g.). In this section we show that the highest velocities are concentrated near the galactic center during the peak of an AGN outburst.

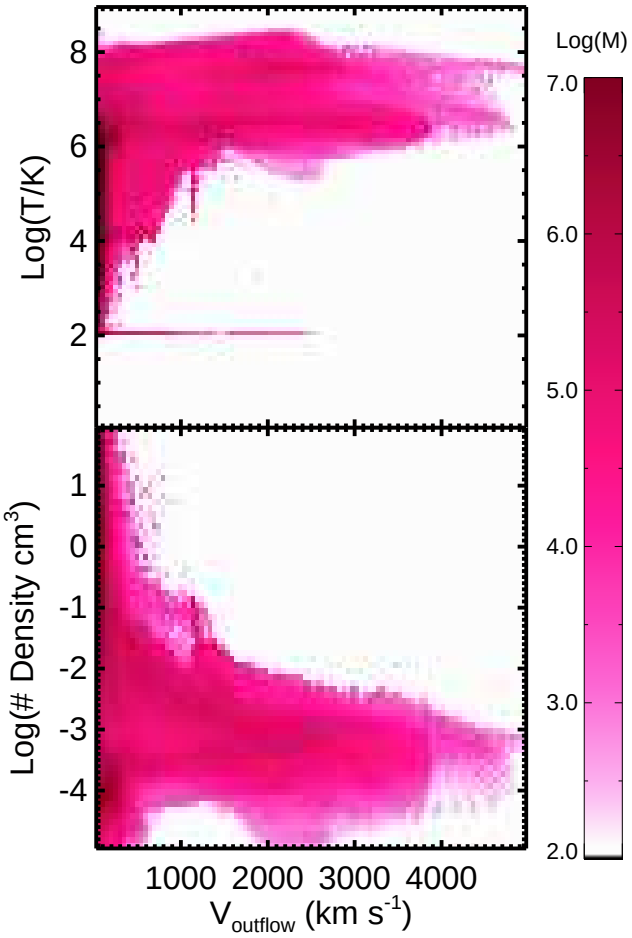

Figure 3. Top: Temperature-velocity diagram for outflowing gas at one snapshot of our simulation. The color of each pixel indicates the mass at that given outflow velocity and temperature, in $M_\odot$. Outflow velocities reach ≈ 5000 km s^{-1}, and most of the high-velocity gas is between 10^6 and 10^8 K. Some of the outflows up to ~ 2500 km s^{-1}are actually at our simulation temperature floor of 100 K. These are probably cold clouds entrained in the hot outflow. **Bottom:** Density-velocity diagram for outflowing gas. Most of the outflowing gas is low-density, below 10^{-2} cm^{-3}, but some gas at 10^{-1} cm^{-3} and denser is outflowing at velocities up to 1000 km s^{-1}.

We measure gas velocity profiles along several lines-of-sight through the galaxy. The lines-of-sight are set up as a square grid with a spacing of 1 kpc between each line-of-sight, which is comparable to the spatial resolution of integral field spectrograph observations of $z \sim 2$ galaxies (e.g. Förster Schreiber et al. 2013). Each line-of-sight passes through the galaxy perpendicular to the galactic disk, emulating a "face-on" observation. We include only gas with temperature $> 10^4$ K (that is also above our temperature floor) to approximate observation of emission-line gas.

Figure 4 shows a map of the maximum outflowing gas velocity at time $t = 6$ Myr of simulation M4f50, during the first major peak of BH accretion. To limit noise induced by small quantities of gas, we actually define the maximum velocity along a given line-of-sight as the highest velocity at which at least 1 per cent of the gas along that line-of-sight

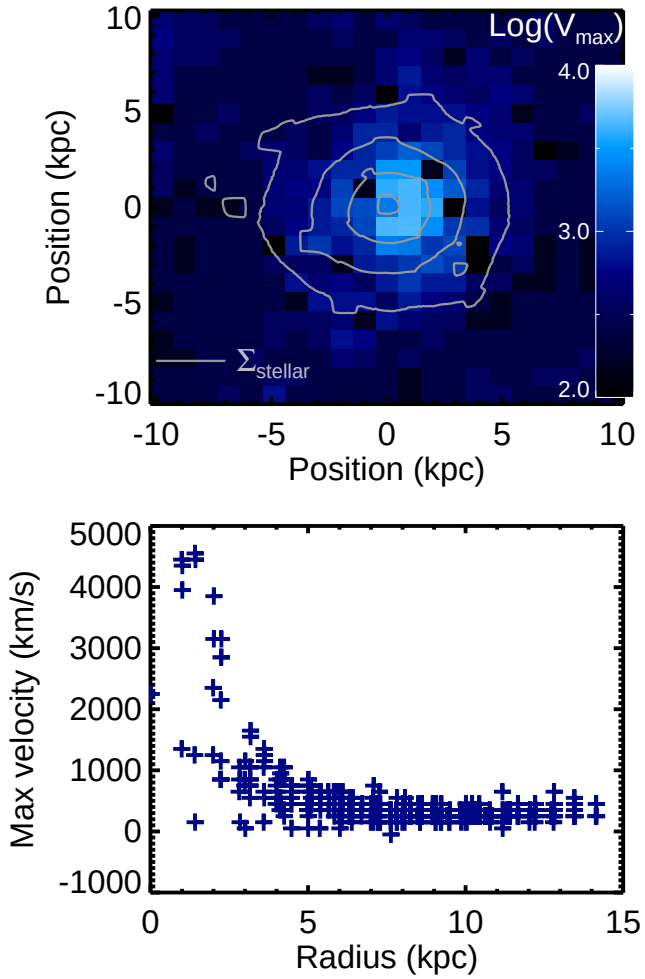

Figure 4. Top: Face-on map of maximum outflow velocity with 1 kpc resolution, at the peak of BH accretion around $t = 6$ Myr. Gray contours indicate the distribution of stellar mass of the galaxy. **Bottom:** Maximum velocity in each pixel from the velocity map above, as a function of the projected distance of the pixel from the galaxy center. During the peak of AGN activity, outflow velocities are highest within $2 - 3$ kpc of the galactic center.

is moving. The lines-of-sight with the highest velocities are concentrated near the galactic center, though the centroid appears somewhat off-center.

In the bottom panel of Figure 4, we show the maximum line-of-sight gas velocity as a function of projected distance between each line-of-sight and the galactic center. The maximum outflow velocity rapidly drops below ~ 1000 km s^{-1}between 2 and 3 kpc from the galactic center. Thus during the peak of AGN activity, the enhanced outflow velocities have an apparent radial extent of $\sim 2 - 3$ kpc.

After the accretion rate declines and the outflow shell expands (cf. Figure 1), high outflow velocities of $\sim$ 3000 are apparent at projected radii out to > 5 kpc. In this case it would be difficult to distinguish an AGN-driven outflow based on high outflow velocities observed near the nucleus. By the time the outflowing shell expands to this size, it may be expected to interact with a more complex circum-galactic medium than that which we model here.

In summary, during the peak of AGN activity, lines-of-sight within $\sim 2-3$ kpc of the galactic center show maximum outflow velocities of several thousand km s^{-1}. Maximum outflow velocities drop rapidly below 1000 km s^{-1}for lines-of-sight at larger radii. This result is somewhat sensitive to the timing – after the accretion rate peak, the outflow shell expands to large radii and high-velocity outflows are visible at large projected radii.

3.5 Effects of AGN feedback on the galaxy

Although AGN outbursts drive peak mass outflow rates near the SFR, and mean outflow rates of a significant fraction of the SFR (Figure 2), they appear to leave the galactic disk intact (cf. Figure 1). In this section we show more explicitly that AGN feedback in our models has little impact on star-forming gas disk.

Figure 5 shows face-on gas density maps of simulations with and without AGN feedback at time $t = 91$ Myr. In detail, AGN feedback alters the evolution of structures within the gas disk. It strips gas from the outskirts of individual dense clouds and may change their dynamics and orbits. But AGN feedback does not generally destroy dense clouds, and the galactic gas disk remains intact. The gas appears to have similar turbulent structure with filaments and dense clouds in both cases.

Figure 6 compares the evolution of dense gas mass for the simulation with AGN feedback to the one without AGN feedback. The two simulations are identical at time zero. In each simulation, we sum the mass of gas above a density of 100 cm^{-3} within 5 kpc of the galactic center. This density is that above which stars may form in our simulations, and also an estimate for the density required to form molecular hydrogen (Gnedin et al. 2009). The dense gas mass declines steadily in both simulations due to gas consumption via star formation and stellar-driven feedback. Both simulations show a small increase in dense gas at $t \approx 70$ Myr, probably due to a massive clump in the outer disk moving within 5 kpc. Remarkably, the simulations with and without AGN feedback have almost identical dense gas mass evolution. The simulation with AGN feedback actually has more dense gas for some of the time, possibly due to compression from the AGN outbursts, but the difference is minor.

Why doesn't the AGN feedback strongly affect the dense gas? Gas cooling rates scale with the square of density, so that when a shock collides with a dense cloud, the added shock energy may be rapidly radiated away (cf. King 2010b). Within the disk plane, dense gas near the AGN effectively shields gas in the outer disk from the effects of the outburst.

In summary, AGN feedback subtly alters details of the gas dynamics in the central disk regions over time, but it primarily affects diffuse gas and does not destroy the disk. The mass of dense gas in the central 5 kpc is essentially unchanged by AGN feedback. In upcoming work we will study how AGN feedback – including ionizing radiation from the central source – affects high-redshift disk galaxy SFRs (Roos et al. in preparation).

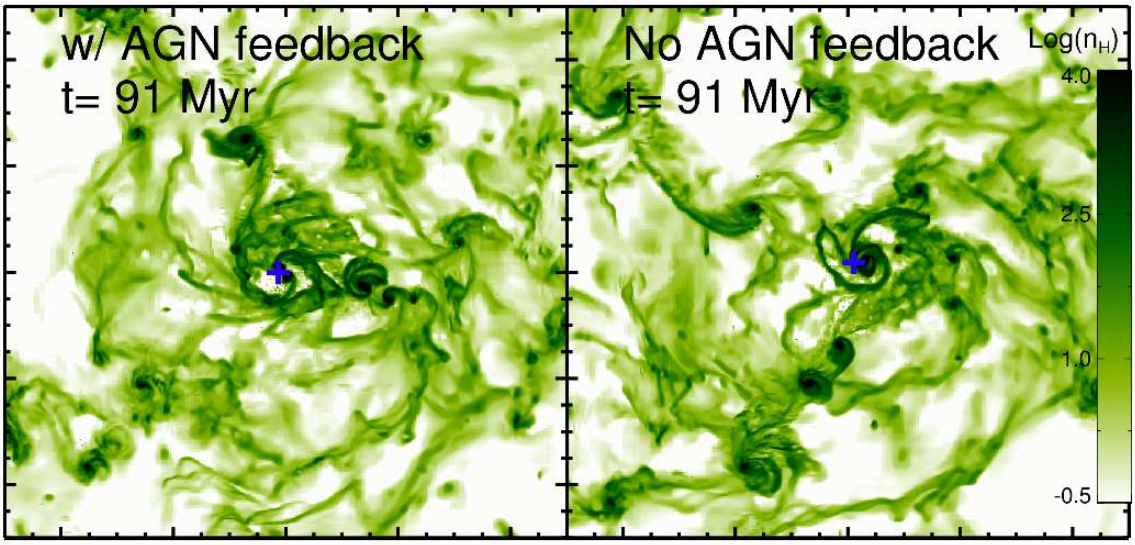

Figure 5. Face-on gas density maps of simulations with (left) and without (right) AGN feedback, at the same simulation time. AGN feedback changes the gas dynamics in detail, affecting the evolution of individual clouds, but it does not destroy the gas disk.

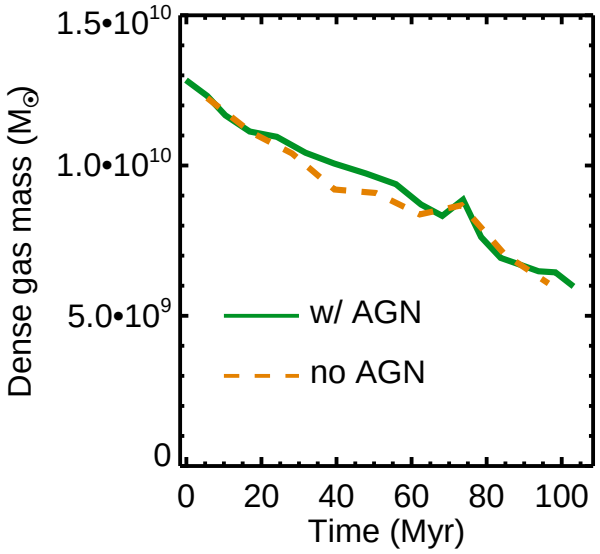

Figure 6. Mass of dense gas ($n_H > 100$ cm−3) within 5 kpc of the galaxy nucleus as a function of time, for simulations with (green solid line) and without (dashed orange) AGN feedback. In both simulations the dense gas content declines as it forms stars, and AGN feedback makes almost no difference.

4 DISCUSSION

4.1 Model-dependence

AGN feedback in our simulations drives bursty, high-velocity, hot outflows with mass rates peaking briefly near the star-formation rate. Recent work suggests that the details of black hole growth and AGN feedback can depend quite strongly on the models for these phenomena (e.g. Nayakshin & Power 2010; Ostriker et al. 2010; Debuhr et al. 2010; Novak et al. 2011; Power et al. 2011; Faucher-Gigu‘ere & Quataert 2012; Anglés-Alcázar et al. 2013; Newton & Kay 2013; Wurster & Thacker 2013b,a). In this section we speculate how our results could be model-dependent, without performing a detailed (and expensive) parameter study.

4.1.1 Dependence on the AGN model

The phase structure of outflows shown in Figure 3 probably depends on the AGN feedback model. Our AGN feedback model operates solely through injection of thermal energy (i.e. by raising the temperature of surrounding gas), and we only inject the energy at temperatures from 10^7 to 5×10^9 K (cf. Booth & Schaye 2009). The characteristic speed corresponding to a thermal temperature of 10^9 K – the sound speed – is ~ 5000 km s^{-1}. Though this is a reasonable velocity for broad absorption line outflows commonly observed in quasars (Trump et al. 2006; Tombesi et al. 2010), we suspect that we could achieve lower-velocity, cooler outflows with higher mass loading by restricting the injection temperature to lower values. That is, one can imagine using the same amount of AGN energy to drive an outflow with kinetic energy $\sim mv^2$, but increasing the mass m and decreasing the velocity v. Some feedback models operate via momentum injection rather than thermal energy injection, and these might produce colder, denser outflows as well (Debuhr et al. 2010).

We tested a straightforward alternative AGN model in which the thermal energy is injected in a volume $5^3 = 125\times$ larger than our default. In this alternative model we still require a minimum temperature of 10^7 K, but the peak temperatures around 10^9 K are rarely reached. This model produces an outflow phase structure that is qualitatively similar to the one shown in Figure 3, including similar outflow velocities. Peak outflow rates, however, are about $2\times$ the ones in Figure 2. This explicitly shows that higher AGN-driven outflow rates are possible with different AGN models.

4.1.2 Dependence on the ISM and stellar feedback models

The "burstiness" of outflows in our simulations arises directly from the highly variable black hole accretion rates (which is common in AGN models; cf. Novak et al. 2011; Hickox et al. 2013), which in turn are driven by structure in the ISM. The ISM structure is sensitive to details of cooling and stellar feedback. Some simulations model a pressurized ISM which tends to be smoother and form fewer dense clouds (e.g. Springel & Hernquist 2003; Di Matteo et al. 2005; Springel et al. 2005). Strong stellar feedback, sometimes involving delayed gas cooling, momentum input, radiation pressure, or cosmic rays, may also help disrupt dense clouds (Genel et al. 2012b; Hopkins et al. 2012a). In our simulations (with weak stellar feedback) the AGN outbursts are fed by dense clouds, so models where these dense clouds are rapidly destroyed could see lower BH accretion rates and thus weaker outbursts. Recent simulations similar to those presented here, but with a sophisticated model for radiation pressure and ionization due to young stars (Renaud et al. 2013), generate strong outflows but appear to leave the clumpy gas structure intact (Perret et al. 2013; Bournaud et al. 2014). Some theoretical work supports the idea that massive clumps should survive strong stellar feedback (Dekel & Krumholz 2013).

4.1.3 Feedback interactions

Along with changing the structure of the ISM, strong stellar feedback can produce outflows (Murray et al. 2005; Oppenheimer & Davé 2006; Dubois et al. 2010b; Murray et al. 2011; Hopkins et al. 2012b; Uhlig et al. 2012; Salem & Bryan 2013). Stellar-driven outflows are (intentionally) weak in our simulations, but the interplay between stellar-driven outflows and AGN-driven outflows may be crucial for understanding how gas is expelled from galaxies. Simulations indicate that different kinds of stellar feedback – radiation pressure from young stars, and supernovae – have a non-linear compounding effect on outflows. That is, the outflow rates with both kinds of feedback simultaneously are higher than the sum of different feedback processes in isolation (Hopkins et al. 2012b). We plan to address this interplay in future work. A related issue is cosmic inflow and the circum-galactic medium. Cosmic inflow may impact the ISM of high-redshift galaxies (Gabor & Bournaud 2013a), and AGN feedback may interact with and even disrupt cold inflows (Dubois et al. 2013b).

4.2 Relation to observations

Our simulations of isolated gas-rich galaxies with AGN-driven outflows can potentially explain some observations of high-velocity outflows. The simulations produce outflow velocities > 1000 km s^{-1}which are often used by observers to attribute outflows to AGN. The peak mass outflow rates of a few tens of $M_\odot$ yr^{-1}, and of order the SFR, are comparable to those estimated from observations (Cicone et al. 2013; Förster Schreiber et al. 2013), though somewhat too small. The outflow size scale of $2-3$ kpc during peak accretion matches observations, though the size increases during the later stages of the flow in our models. The rapid variability of the AGN combined with the time lag of the outflow may explain observations of high-velocity outflows in the absence of AGN signatures (Diamond-Stanic et al. 2012; Förster Schreiber et al. 2013).

Other aspects of observed outflows may be difficult to explain with our model. The gas in our simulations is probably hotter than in observations, although such outflowing hot gas may exist undetected in real galaxies. Our model does not produce much cold, dense outflowing gas, while observations indicate that dense molecular gas ($\gtrsim 100$ cm^{-3}) is outflowing at high velocities along with ionized gas. This discrepancy could be due to cooling on scales that our simulation does not resolve. Although our peak resolution is ~ 6 pc, our adaptive refinement strategy only applies such high resolution to the densest gas in the galactic disk. Alternatively, the lack of cold dense outflows in our model could be due to inadequacies in the model used to generate the outflows.

Future work could benefit from synthetic observations of simulated outflows. The hot outflows in our simulations would be highly ionized and emit in X-rays. Radiative transfer calculations could assess the observability of various ionization species' emission and absorption lines and the X-ray continuum. They could also help calibrate the connection between direct observables, such as emission line widths and shapes, and physical outflow properties such as outflow rates.

4.3 AGN outflows without quenching star-formation

Some authors interpret observed high-velocity AGN outflows as a mechanism for quenching star-formation. In our models, the AGN has little effect on the gas reservoir in the disk of the galaxy. If real AGN are highly variable, as in our simulations, then time-averaged outflow rates may be significantly lower than instantaneously observed outflow rates.

Instead of quenching star-formation, we interpret AGN outflows from disk galaxies as contributing to the overall galactic outflow. Observations and models suggest that (stellar-driven) galactic outflow rates of $\gtrsim 2$ times the SFR are reasonable (Murray et al. 2005; Erb et al. 2006; Oppenheimer & Davé 2006; Weiner et al. 2009; Bouché et al. 2012; Davé et al. 2012; Newman et al. 2012), but these do not quench star-formation because galaxies are constantly fed additional fuel from the IGM. Indeed, the key physical element required to produce a galaxy red sequence is not to expel gas from galaxies, but rather to prevent gas from entering galaxies in the first place (Bower et al. 2006; Croton et al. 2006; Hopkins et al. 2008; Gabor et al. 2011). In continuity or equilibrium galaxy evolution models the intergalactic inflows are roughly balanced by star-formation and outflows over most of cosmic history: $\dot{M}_{\rm inflow} \approx \dot{M}_{\rm SFR} + \dot{M}_{\rm outflow}$ (Bouché et al. 2010; Davé et al. 2012; Genel et al. 2012a; Lilly et al. 2013; Dekel et al. 2013). Based on our simulations, AGN may contribute a significant (but sub-dominant) fraction of the outflows, $\dot{M}_{\rm outflow} = \dot{M}_{\rm outflow,stars} + \dot{M}_{\rm outflow,AGN}$, rather than quenching star-formation.

Perhaps the story differs for high-mass star-forming galaxies. Observations suggest a high fraction of high-mass $z \sim 2$ galaxies show signatures of AGN-driven outflows (Förster Schreiber et al. 2013), implying a higher outflow

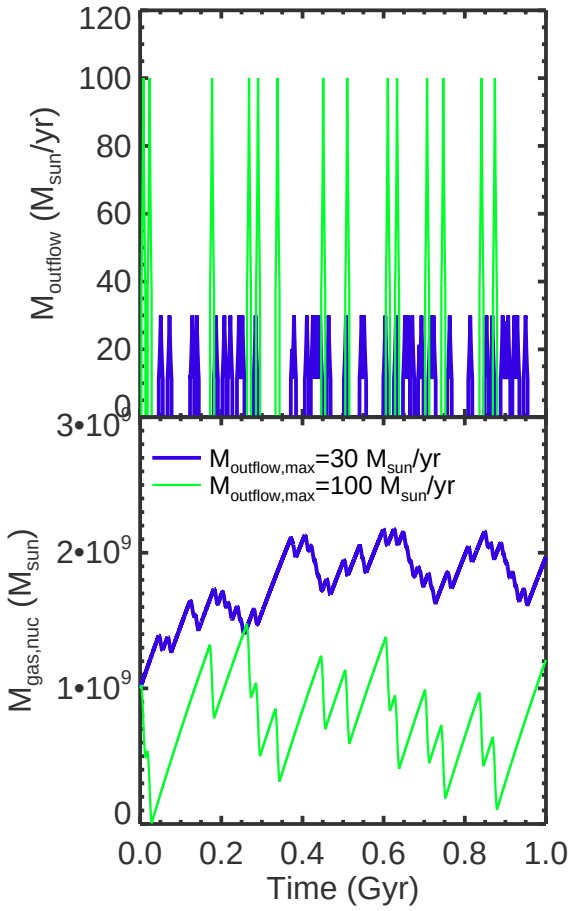

Figure 7. Evolution of a toy model for nuclear outflows. **Top:** Mass outflow rates are driven to large values during brief, stochastic AGN outbursts. Here we consider two cases of maximum outflow rates: 30 $M_\odot$ yr^{-1}(blue lines) and 100 $M_\odot$ yr^{-1}(green lines). **Bottom:** The nuclear gas mass fluctates with inflows from the galactic disk and outflows driven by the AGN outbursts. Even with high outflow rates, the nucleus spends little time devoid of gas. Note the total galactic gas mass is about 10× higher than the nuclear gas mass, and remains roughly constant with time – it is essentially unaffected by AGN feedback.

duty cycle. These galaxies may have more massive bulges and black holes, so at any given Eddington ratio the AGN is more powerful, potentially driving a more massive outflow. Could these observed AGN-driven outflows ultimate expel all the gas from the galaxy? Future simulations with higher bulge and BH masses could help elucidate the situation.

4.3.1 A toy model of nuclear outflows

To illustrate AGN outflows without quenching, we outline here a toy bathtub-in-a-bathtub model, the key features of which are based on our simulation results. The black hole accretes from gas in the nuclear region, and in our simulations AGN feedback only affects the gas in the nuclear region, say the central kpc. Therefore, we treat the nucleus as a nearly-independent gas reservoir, connected to the rest of the galaxy disk only through inflows from the disk to the nucleus. Bournaud et al. (2011) estimate the inflow toward the nucleus of an unstable gaseous disk galaxy as $\dot{M}_{\rm inflow,nuc} = 0.2(M_{\rm disk}/t_{\rm d})(\sigma/V)^2$, where $M_{\rm disk}$ is the total galaxy disk mass, $t_{\rm d}$ is the disk dynamical time, σ is the velocity dispersion, and V is the characteristic rotation speed. For a galaxy like our main simulation, this gives $\dot{M}_{\rm inflow,nuc} \approx 10$ $M_\odot$ yr^{-1}.

Gas sink terms from this nuclear region include star-formation, accretion onto the black hole, gas ejected by stellar feedback, and gas ejected by AGN feedback. The star-formation rate is $\dot{M}_{\rm SFR,nuc} = M_{\rm nuc}/t_{\rm SFR}$, where $M_{\rm nuc}$ is the gas mass in the nuclear region, and $t_{\rm SFR} = 800$ Myr. We neglect accretion onto the black hole and stellar feedback since they are sufficiently small in our simulations that including them would not substantially change the result. AGN-driven outflows are treated as stochastic bursts. At any given time a new outburst can begin, with a probability of $0.01M_{\rm nuc}/M_{\rm crit}$, and we choose $M_{\rm crit} = 5 \times 10^9$ $M_\odot$. Outflow rates rise for a time $0.5dt_{\rm burst}$ as $\dot{M}_{\rm outflow} = \dot{M}_{\rm out,max} \exp((t - t_{\rm burst} - 0.5dt_{\rm burst})/\tau_{\rm burst})$, peak at $\dot{M}_{\rm out,max}$, then decline as $\dot{M}_{\rm outflow} = \dot{M}_{\rm out,max} \exp(-(t - t_{\rm burst} - 0.5dt_{\rm burst})/\tau_{\rm burst})$. Here, $dt_{\rm burst} = 10$ Myr is the length of each AGN outburst, $\tau_{\rm burst} = 5$ Myr is an exponential growth/decay timescale for the outflow rate, t is the time, and $t_{\rm burst}$ is the time at which the burst began. Outside of the bursts, outflow rates are assumed to be zero.

This nuclear reservoir is embedded in the broader reservoir of the galaxy disk. This larger gas reservoir gains mass from cosmic accretion, and loses mass to star-formation, star-formation driven outflows, and inflows to the nucleus: $\dot{M}_{\rm gas,disk} = \dot{M}_{\rm inflow,cosmic} - \dot{M}_{\rm SFR,disk} - \dot{M}_{\rm outflow,disk} - \dot{M}_{\rm inflow,nuc}$, where $\dot{M}_{\rm inflow,cosmic} = 60$ $M_\odot$ yr^{-1}is the intergalactic inflow into the galaxy, $\dot{M}_{\rm SFR,disk} = M_{\rm gas,disk}/t_{\rm SFR}$ is the star-formation rate in the disk, and $\dot{M}_{\rm outflow,disk} = \dot{M}_{\rm SFR,disk}$ is the stellar-driven outflow rate from the disk. With the parameter choices above, the gas mass (and thus the star-formation rate) of the disk remains constant over time, as is roughly the case for $z \sim 2$ galaxies in equilibrium models of galaxy evolution (e.g. Davé et al. 2012; Genel et al. 2012a; Lilly et al. 2013; Dekel et al. 2013).

Figure 7 shows the AGN-driven outflow rates and nuclear gas masses for two example numerical solutions of the above equations over 1 Gyr – one case with $\dot{M}_{\rm out,max} = 30$ $M_\odot$ yr^{-1}(blue), and one with $\dot{M}_{\rm out,max} = 100$ $M_\odot$ yr^{-1}(green). The top panel shows the mass outflow rate $\dot{M}_{\rm outflow}$ due to the stochastic, sharp AGN outbursts. The bottom panel shows the nuclear gas mass, $M_{\rm nuc}$. The nuclear gas mass increases due to the disk inflow, and decreases during AGN outbursts. Even in the case with high mass outflow rates, the nuclear region is occasionally cleared of most of its gas, but additional gas inflows quickly rebuild the nuclear reservoir. This model captures the hallmark of black hole self-regulation – when AGN outbursts rid the nuclear region of gas, there is no fuel to trigger an AGN, so more gas is allowed to build up.

While this toy model ignores some details (e.g. variability in the inflow rate, ionizing radiation from the central source; Roos et al. in preparation), it illustrates frequent and episodic strong outflows *without* quenching. The AGN empties the gas only from the nuclear region, leaving the galaxy disk intact. The nuclear region is replenished rapidly

due to instability-driven gas inflows, ultimately triggering additional AGN and more outflows. Thus the nucleus persists in a quasi-steady state where AGN-driven outflows are roughly balanced on long time scales by gas inflows, despite variability on $\sim$ Myr time scales. Since the SFR of the galaxy is dominated by the disk, not the nucleus, the total instantaneous SFR is practically unaffected by AGN feedback. Over long time scales, a substantial amount of gas may be ejected from the galaxy by AGN feedback, but this does not "quench" star-formation because the galaxy accretes new gas. Generally, nuclei and galaxies with an ongoing source of cold gas will not be quenched even in the presence of strong outflows.

5 SUMMARY AND CONCLUSION

We have studied AGN-driven outflows using a small suite of simulations of gas-rich, high-redshift isolated disk galaxies. The main results from our simulations are:

- AGN outbursts occur in short, episodic bursts lasting $\sim 5 - 10$ Myr.
- AGN feedback drives high-velocity outflows with mass outflow rates peaking near the SFR (a few 10's of $M_\odot$ yr^{-1}). The time-averaged outflow rate can be $\sim 1/3$ of the SFR.
- Dense gas in the galactic disk directs AGN outflows out of the plane of the disk. The outflows propagate into the circum-galactic region as semi-spherical blast waves.
- AGN outflows are frequently asymmetric, expanding only above or below the gas disk, not both. Dense gas clouds vertically offset from the central engine can block the outflow in some directions.
- AGN outflows are predominantly hot and diffuse ($T \sim 10^7$ K and $n_H \sim 10^{-3}$ cm^{-3}), but some colder, denser clouds ($T \sim 10^2 - 10^4$ K and $n_H \sim 10^{-1}$ cm^{-3}) are swept up in the hot outflows.
- During peak BH accretion, the highest outflow velocities are visible along lines-of-sight within $2 - 3$ kpc of the galactic center.
- AGN feedback has only a weak effect on the detailed dynamics of the galaxy's gas. The mass of dense gas in the disk is almost identical for simulations with and without AGN feedback.

Beyond these main points, we have speculated on how these results could be model-dependent, and we have discussed their relation to observations and the popular idea of AGN-driven quenching. We advocate a picture where typical AGN-driven outflows contribute to the overall galactic outflows, but do not affect the dense gas in the disk or the SFR. AGNs fueled by disk instabilities exist in a quasi-steady state where powerful outflow bursts balance nuclear inflows over long timescales, without quenching star-formation across the galaxy disk.

ACKNOWLEDGEMENTS

We thank Romain Teyssier for making RAMSES available. We acknowledge support from the EC through grants ERC-StG-257720 and the CosmoComp ITN. Simulations were performed at TGCC and as part of a GENCI project (grants 2011-042192, 2012-042192, and 2013-042192).

REFERENCES

Aalto S., Garcia-Burillo S., Muller S., Winters J. M., van der Werf P., Henkel C., Costagliola F., Neri R., 2012, A&A, 537, A44
Alatalo K. et al., 2011, ApJ, 735, 88
Anglés-Alcázar D., Özel F., Davé R., Katz N., Kollmeier J. A., Oppenheimer B. D., 2013, ArXiv e-prints
Begelman M. C., Nath B. B., 2005, MNRAS, 361, 1387
Bennert N., Canalizo G., Jungwiert B., Stockton A., Schweizer F., Peng C. Y., Lacy M., 2008, ApJ, 677, 846
Bennert V. N., Auger M. W., Treu T., Woo J.-H., Malkan M. A., 2011, ApJ, 726, 59
Bessiere P. S., Tadhunter C. N., Ramos Almeida C., Villar Martín M., 2012, MNRAS, 426, 276
Bondi H., 1952, MNRAS, 112, 195
Bondi H., Hoyle F., 1944, MNRAS, 104, 273
Booth C. M., Schaye J., 2009, MNRAS, 398, 53
Bouché N. et al., 2010, ApJ, 718, 1001
Bouché N., Hohensee W., Vargas R., Kacprzak G. G., Martin C. L., Cooke J., Churchill C. W., 2012, MNRAS, 426, 801
Bournaud F., Dekel A., Teyssier R., Cacciato M., Daddi E., Juneau S., Shankar F., 2011, ApJ, 741, L33
Bournaud F. et al., 2014, ApJ, 780, 57
Bower R. G., Benson A. J., Malbon R., Helly J. C., Frenk C. S., Baugh C. M., Cole S., Lacey C. G., 2006, MNRAS, 370, 645
Cales S. L. et al., 2011, ApJ, 741, 106
Canalizo G., Wold M., Hiner K. D., Lazarova M., Lacy M., Aylor K., 2012, ApJ, 760, 38
Cano-Díaz M., Maiolino R., Marconi A., Netzer H., Shemmer O., Cresci G., 2012, A&A, 537, L8
Ceverino D., Dekel A., Bournaud F., 2010, MNRAS, 404, 2151
Cicone C., Feruglio C., Maiolino R., Fiore F., Piconcelli E., Menci N., Aussel H., Sturm E., 2012, A&A, 543, A99
Cicone C. et al., 2013, ArXiv e-prints
Ciotti L., Ostriker J. P., 1997, ApJ, 487, L105
—, 2001, ApJ, 551, 131
Ciotti L., Ostriker J. P., Proga D., 2010, ApJ, 717, 708
Cisternas M. et al., 2011, ApJ, 726, 57
Croton D. J. et al., 2006, MNRAS, 365, 11
Davé R., Finlator K., Oppenheimer B. D., 2012, MNRAS, 421, 98
Debuhr J., Quataert E., Ma C.-P., 2012, MNRAS, 420, 2221
Debuhr J., Quataert E., Ma C.-P., Hopkins P., 2010, MNRAS, 406, L55
Dekel A., Krumholz M. R., 2013, MNRAS, 432, 455
Dekel A., Sari R., Ceverino D., 2009, ApJ, 703, 785
Dekel A., Zolotov A., Tweed D., Cacciato M., Ceverino D., Primack J. R., 2013, MNRAS, 435, 999
Di Matteo T., Springel V., Hernquist L., 2005, Nature, 433, 604
Diamond-Stanic A. M., Moustakas J., Tremonti C. A., Coil A. L., Hickox R. C., Robaina A. R., Rudnick G. H., Sell P. H., 2012, ApJ, 755, L26
Dubois Y., Devriendt J., Slyz A., Teyssier R., 2010a, MNRAS, 409, 985
—, 2010b, MNRAS, 409, 985
—, 2012, MNRAS, 420, 2662

Dubois Y., Gavazzi R., Peirani S., Silk J., 2013a, MNRAS, 433, 3297
Dubois Y., Pichon C., Devriendt J., Silk J., Haehnelt M., Kimm T., Slyz A., 2013b, MNRAS, 428, 2885
Eddington A. S., 1916, MNRAS, 77, 16
Erb D. K., Shapley A. E., Pettini M., Steidel C. C., Reddy N. A., Adelberger K. L., 2006, ApJ, 644, 813
Fabian A. C., 1999, MNRAS, 308, L39
Faucher-Gigu'ere C.-A., Quataert E., 2012, MNRAS, 425, 605
Ferrarese L., Merritt D., 2000, ApJ, 539, L9
Feruglio C., Maiolino R., Piconcelli E., Menci N., Aussel H., Lamastra A., Fiore F., 2010, A&A, 518, L155+
Förster Schreiber N. M. et al., 2013, ArXiv e-prints
Gabor J. M., Bournaud F., 2013a, MNRAS
—, 2013b, MNRAS, 434, 606
Gabor J. M., Davé R., Oppenheimer B. D., Finlator K., 2011, MNRAS, 417, 2676
Gabor J. M. et al., 2009, ApJ, 691, 705
Gebhardt K. et al., 2000, ApJ, 539, L13
Genel S., Dekel A., Cacciato M., 2012a, MNRAS, 425, 788
Genel S., Naab T., Genzel R., Förster Schreiber N. M., Sternberg A., Oser L., Johansson P. H., Davé R., Oppenheimer B. D., Burkert A., 2012b, ApJ, 745, 11
Georgakakis A. et al., 2009, MNRAS, 397, 623
Gnedin N. Y., Tassis K., Kravtsov A. V., 2009, ApJ, 697, 55
González-Alfonso E. et al., 2013, ArXiv e-prints
Graham A. W., 2007, MNRAS, 379, 711
Graham A. W., Scott N., 2013, ApJ, 764, 151
Grogin N. A. et al., 2005, ApJ, 627, L97
Haehnelt M. G., Natarajan P., Rees M. J., 1998, MNRAS, 300, 817
Harrison C. M. et al., 2012, MNRAS, 426, 1073
Hickox R. C., Mullaney J. R., Alexander D. M., Chen C.-T. J., Civano F. M., Goulding A. D., Hainline K. N., 2013, ArXiv e-prints
Hopkins P. F., Cox T. J., Kereš D., Hernquist L., 2008, ApJS, 175, 390
Hopkins P. F., Hernquist L., 2006, ApJS, 166, 1
Hopkins P. F., Hernquist L., Cox T. J., Di Matteo T., Robertson B., Springel V., 2006, ApJS, 163, 1
Hopkins P. F., Kereš D., Murray N., Quataert E., Hernquist L., 2012a, MNRAS, 427, 968
Hopkins P. F., Kocevski D. D., Bundy K., 2013, ArXiv e-prints
Hopkins P. F., Quataert E., Murray N., 2012b, MNRAS, 421, 3522
—, 2012c, MNRAS, 421, 3488
Hoyle F., Lyttleton R. A., 1939, in Proceedings of the Cambridge Philosophical Society, Vol. 35, Proceedings of the Cambridge Philosophical Society, pp. 405–+
Jahnke K. et al., 2009, ApJ, 706, L215
Juneau S. et al., 2013, ApJ, 764, 176
Katz N., Weinberg D. H., Hernquist L., 1996, ApJS, 105, 19
King A., 2005, ApJ, 635, L121
King A. R., 2010a, MNRAS, 408, L95
—, 2010b, MNRAS, 402, 1516
Kocevski D. D. et al., 2012, ApJ, 744, 148
Kormendy J., Ho L. C., 2013, ARA&A, 51, 511
Kormendy J., Richstone D., 1995, ARA&A, 33, 581
Krumholz M. R., McKee C. F., Klein R. I., 2004, ApJ, 611, 399
Krumholz M. R., Tan J. C., 2007, ApJ, 654, 304
Lehnert M. D., Tasse C., Nesvadba N. P. H., Best P. N., van Driel W., 2011, A&A, 532, L3
Lilly S. J., Carollo C. M., Pipino A., Renzini A., Peng Y., 2013, ApJ, 772, 119
Magorrian J. et al., 1998, AJ, 115, 2285
Maiolino R. et al., 2012, MNRAS, 425, L66
Marconi A., Hunt L. K., 2003, ApJ, 589, L21
Martizzi D., Teyssier R., Moore B., 2012, MNRAS, 420, 2859
McLure R. J., Dunlop J. S., 2002, MNRAS, 331, 795
Mullaney J. R. et al., 2012, ApJ, 753, L30
Murray N., Ménard B., Thompson T. A., 2011, ApJ, 735, 66
Murray N., Quataert E., Thompson T. A., 2005, ApJ, 618, 569
Nayakshin S., Power C., 2010, MNRAS, 402, 789
Nesvadba N. P. H., Polletta M., Lehnert M. D., Bergeron J., De Breuck C., Lagache G., Omont A., 2011, MNRAS, 415, 2359
Newman S. F. et al., 2012, ApJ, 761, 43
Newton R. D. A., Kay S. T., 2013, ArXiv e-prints
Novak G. S., Ostriker J. P., Ciotti L., 2011, ApJ, 737, 26
Oppenheimer B. D., Davé R., 2006, MNRAS, 373, 1265
Ostriker J. P., Choi E., Ciotti L., Novak G. S., Proga D., 2010, ApJ, 722, 642
Peng C. Y., Impey C. D., Rix H.-W., Kochanek C. S., Keeton C. R., Falco E. E., Lehár J., McLeod B. A., 2006, ApJ, 649, 616
Perret V., Renaud F., Epinat B., Amram P., Bournaud F., Contini T., Teyssier R., Lambert J.-C., 2013, ArXiv e-prints
Pierce C. M. et al., 2007, ApJ, 660, L19
Power C., Nayakshin S., King A., 2011, MNRAS, 412, 269
Ramos Almeida C. et al., 2012, MNRAS, 419, 687
Rasera Y., Teyssier R., 2006, A&A, 445, 1
Renaud F. et al., 2013, ArXiv e-prints
Richstone D. et al., 1998, Nature, 395, A14+
Robertson B., Hernquist L., Cox T. J., Di Matteo T., Hopkins P. F., Martini P., Springel V., 2006, ApJ, 641, 90
Rosario D. J. et al., 2012, A&A, 545, A45
Rupke D. S. N., Veilleux S., 2011, ApJ, 729, L27
—, 2013, ApJ, 768, 75
Salem M., Bryan G. L., 2013, MNRAS
Sazonov S. Y., Ostriker J. P., Ciotti L., Sunyaev R. A., 2005, MNRAS, 358, 168
Schawinski K., Simmons B. D., Urry C. M., Treister E., Glikman E., 2012, MNRAS, 425, L61
Silk J., Rees M. J., 1998, A&A, 331, L1
Silverman J. D. et al., 2009, ApJ, 696, 396
Simmons B. D., Urry C. M., Schawinski K., Cardamone C., Glikman E., 2012, ApJ, 761, 75
Somerville R. S., Hopkins P. F., Cox T. J., Robertson B. E., Hernquist L., 2008, MNRAS, 391, 481
Spoon H. W. W. et al., 2013, ApJ, 775, 127
Springel V., Di Matteo T., Hernquist L., 2005, ApJ, 620, L79
Springel V., Hernquist L., 2003, MNRAS, 339, 289
Stinson G., Seth A., Katz N., Wadsley J., Governato F., Quinn T., 2006, MNRAS, 373, 1074

Sutherland R. S., Dopita M. A., 1993, ApJS, 88, 253
Teyssier R., 2002, A&A, 385, 337
Teyssier R., Moore B., Martizzi D., Dubois Y., Mayer L., 2011, MNRAS, 414, 195
Teyssier R., Pontzen A., Dubois Y., Read J. I., 2013, MNRAS, 429, 3068
Tombesi F., Cappi M., Reeves J. N., Palumbo G. G. C., Yaqoob T., Braito V., Dadina M., 2010, A&A, 521, A57
Treister E., Schawinski K., Urry C. M., Simmons B. D., 2012, ApJ, 758, L39
Tremaine S. et al., 2002, ApJ, 574, 740
Tremonti C. A., Moustakas J., Diamond-Stanic A. M., 2007, ApJ, 663, L77
Treu T., Malkan M. A., Blandford R. D., 2004, ApJ, 615, L97
Treu T., Woo J.-H., Malkan M. A., Blandford R. D., 2007, ApJ, 667, 117
Truelove J. K., Klein R. I., McKee C. F., Holliman II J. H., Howell L. H., Greenough J. A., 1997, ApJ, 489, L179
Trump J. R. et al., 2006, ApJS, 165, 1
Uhlig M., Pfrommer C., Sharma M., Nath B. B., Enßlin T. A., Springel V., 2012, MNRAS, 423, 2374
Veilleux S. et al., 2013, ApJ, 776, 27
Weiner B. J. et al., 2009, ApJ, 692, 187
Wurster J., Thacker R. J., 2013a, MNRAS, 431, 2513
—, 2013b, MNRAS, 431, 539
Wyithe J. S. B., Loeb A., 2003, ApJ, 595, 614